CHARACTERIZING THE EDGE PLASMA OF DIFFERENT OHMIC CONFINEMENT REGIMES IN ASDEX

Monika Bessenrodt-Weberpals, Arthur Carlson,
Günter Haas, Heindieter Murmann,
Josef Neuhauser, Franz-Xaver Söldner,
Nikos Tsois*, Henning Verbeek
and the ASDEX Team

IPP 1/248 May 1989

MAX-PLANCK-INSTITUT FÜR PLASMAPHYSIK

8046 GARCHING BEI MÜNCHEN

MAX-PLANCK-INSTITUT FÜR PLASMAPHYSIK

GARCHING BEI MÜNCHEN

CHARACTERIZING THE EDGE PLASMA OF DIFFERENT OHMIC CONFINEMENT REGIMES IN ASDEX

Monika Bessenrodt-Weberpals, Arthur Carlson,
Günter Haas, Heindieter Murmann,
Josef Neuhauser, Franz-Xaver Söldner,
Nikos Tsois*, Henning Verbeek
and the ASDEX Team

IPP 1/248 May 1989

*N.R.C.N.S. Democritos, Athens, Greece

Die nachstehende Arbeit wurde im Rahmen des Vertrages zwischen dem Max-Planck-Institut für Plasmaphysik und der Europäischen Atomgemeinschaft über die Zusammenarbeit auf dem Gebiete der Plasmaphysik durchgeführt.

Abstract

To compare different ohmic confinement regimes in ASDEX, the edge conditions are analyzed in detail. The results show that the improved ohmic confinement comes along with a drop of the separatrix density. This drop allows the density profile to peak and seems to be the trigger of a change in the transport. Simultaneously, a universal scaling between the electron temperature and the electron density at the separatrix prevails for all ohmic scenarios. In addition, the total particle flux across the separatrix is evaluated and found to be strongly correlated to the separatrix density. Thus, the associated convective energy loss contributes less to the total energy losses when the confinement is improved. Since the correlations between edge parameters do not change in different ohmic confinement regimes of ASDEX, the edge physics remains about the same. Improved ohmic confinement is then characterized by an optimum separatrix density which provides a sufficient high edge temperature together with low particle fluxes. These optimum conditions then yield the maximum particle confinement.

PACS numbers : 52.50, 52.55, 52.70.

1. Introduction

The edge conditions play a crucial role in achieving and maintaining the improved ohmic confinement (IOC) regime in ASDEX as has been stated by Haas et al. (1988) and Söldner et al. (1988). This new regime is obtained in deuterium discharges after divertor reconstruction. To achieve long pulse heating, the titanium target plates have been replaced by water-cooled copper target plates and the divertor chamber itself has been narrowed by water-cooled stainless steel shields (Niedermeyer et al., 1988). The new geometry is sketched in Figure 1. IOC is then characterized by the linear scaling of the energy confinement time τ_E with the line-averaged density $\overline{n}_e$ which is recovered at high densities up to the density limit. Typical for the IOC regime are the peaked density profiles. Apart from the H mode a peaked density profile is a commen feature of all regimes with improved confinement in ASDEX like the counter injection (Gehre et al., 1988) and the pellet injection (Kaufmann et al., 1988).

In this paper, we discuss the evolution of the *edge* parameters in different ohmic confinement regimes of ASDEX from the linear (LOC) to the saturated (SOC) and then to the improved (IOC) ohmic regime. In addition, we describe the edge plasma mainly in terms of edge parameters like the *separatrix* density instead of bulk parameters such as the *line-averaged* density. This gives us the opportunity to identify edge effects and to separate them from the central behaviour.

The electron density n_s and temperature T_s in the vicinity of the separatrix are obtained from the single-pulse edge Thomson scattering system and the outermost channel of the quasi-continuous bulk Thomson scattering with an accuracy of 20 % for n_s and 15 % for T_s. Additionally, the time-of-flight spectrometer LENA measures the mean energy and the particle flux of CX hydrogen neutrals in the edge of ASDEX. In the divertor chamber, the electron parameters are determined by Langmuir triple probes with an accuracy of about 25 %. There, various ionization gauges with different configurations are used to measure either the density or the fluxes of hydrogen molecules.

The comparison of different edge diagnostics then suffers from the fact that the separatrix position in the midplane is determined by magnetic probes with an accuracy of only $\pm$ 1 cm. This value is comparable to the radial e-folding lengths

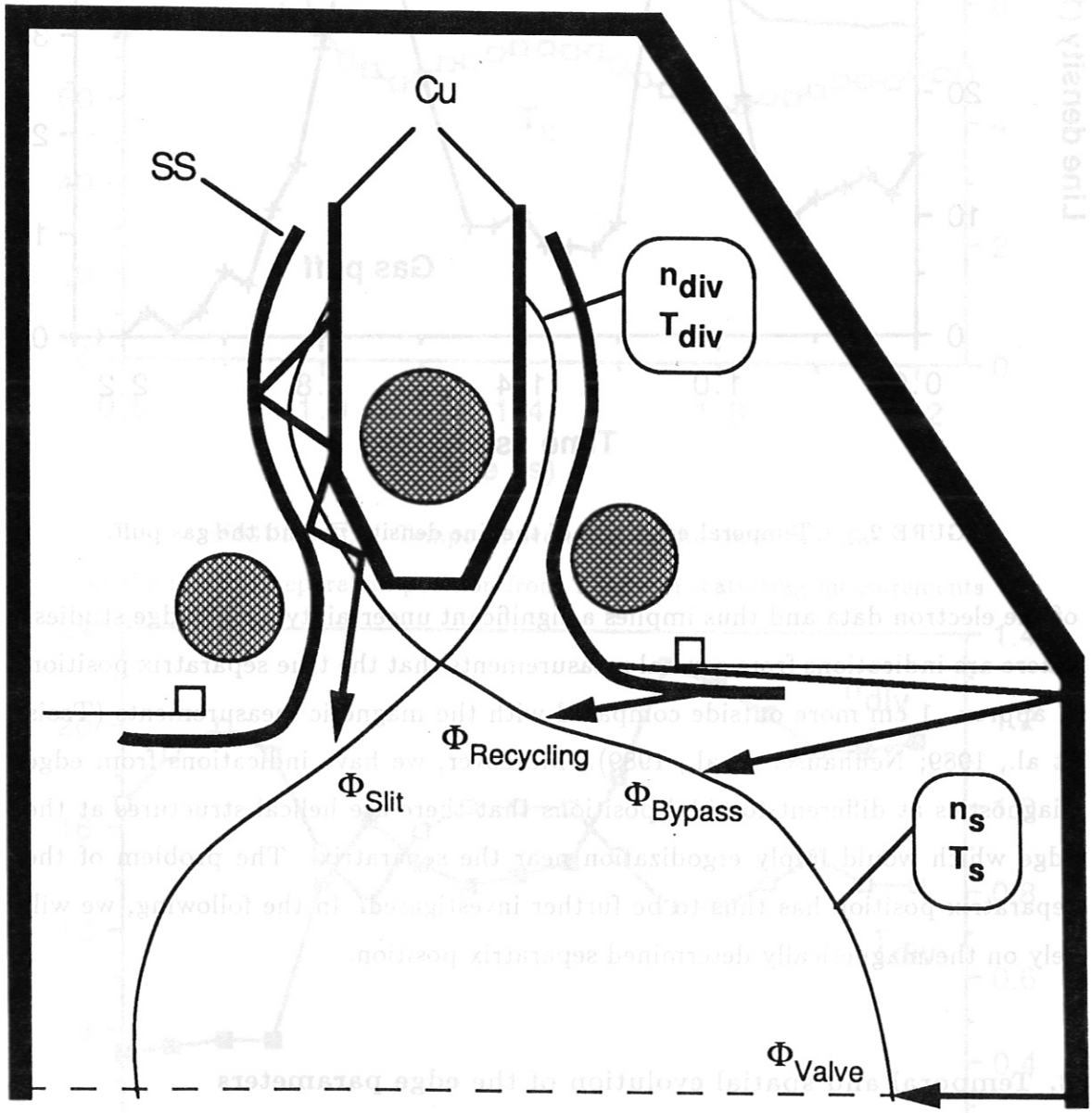

FIGURE 1 : Geometry of the ASDEX divertor configuration DV-II.

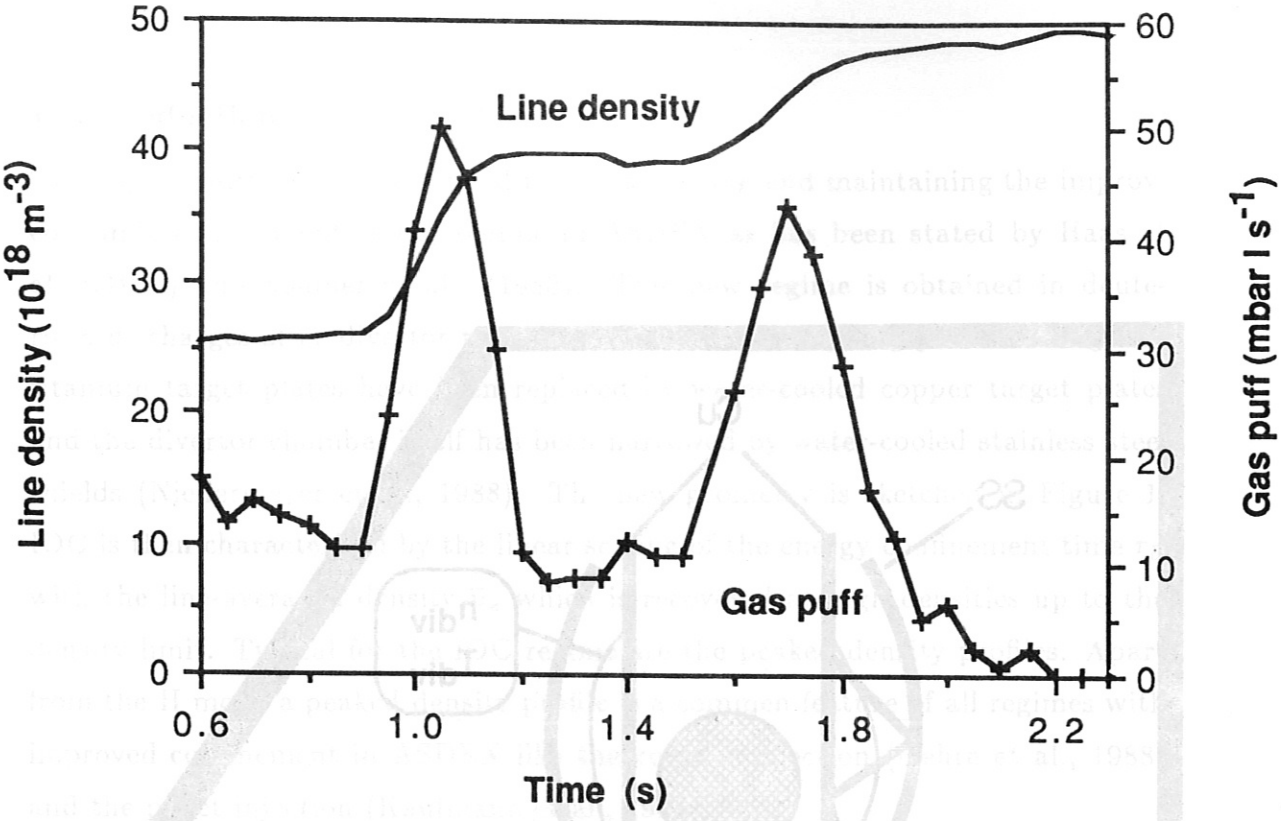

FIGURE 2 : Temporal evolution of the line density $\overline{n}_e$ and the gas puff.

of the electron data and thus implies a significant uncertainty for all edge studies. There are indications from several measurements that the true separatrix position is approx. 1 cm more outside compared with the magnetic measurements (Tsois et al., 1989; Neuhauser et al., 1989). Moreover, we have indications from edge diagnostics at different toroidal positions that there are helical structures at the edge which would imply ergodization near the separatrix. The problem of the separatrix position has thus to be further investigated. In the following, we will rely on the magnetically determined separatrix position.

2. Temporal and spatial evolution of the edge parameters

To get detailed information about the temporal evolution of the SOC to IOC transition in ASDEX we study a lot of scenarios. In one typical example, we build up the density with successive plateaus at $\overline{n}_e = 2.5 \times 10^{19}$ m^{-3} (LOC), $\overline{n}_e = 4.0 \times 10^{19}$ m^{-3} (IOC1), and $\overline{n}_e = 4.9 \times 10^{19}$ m^{-3} (IOC2) each separated by a linear density ramp (SOC1, SOC2) (cf. Figure 2). To this aim, we change the external

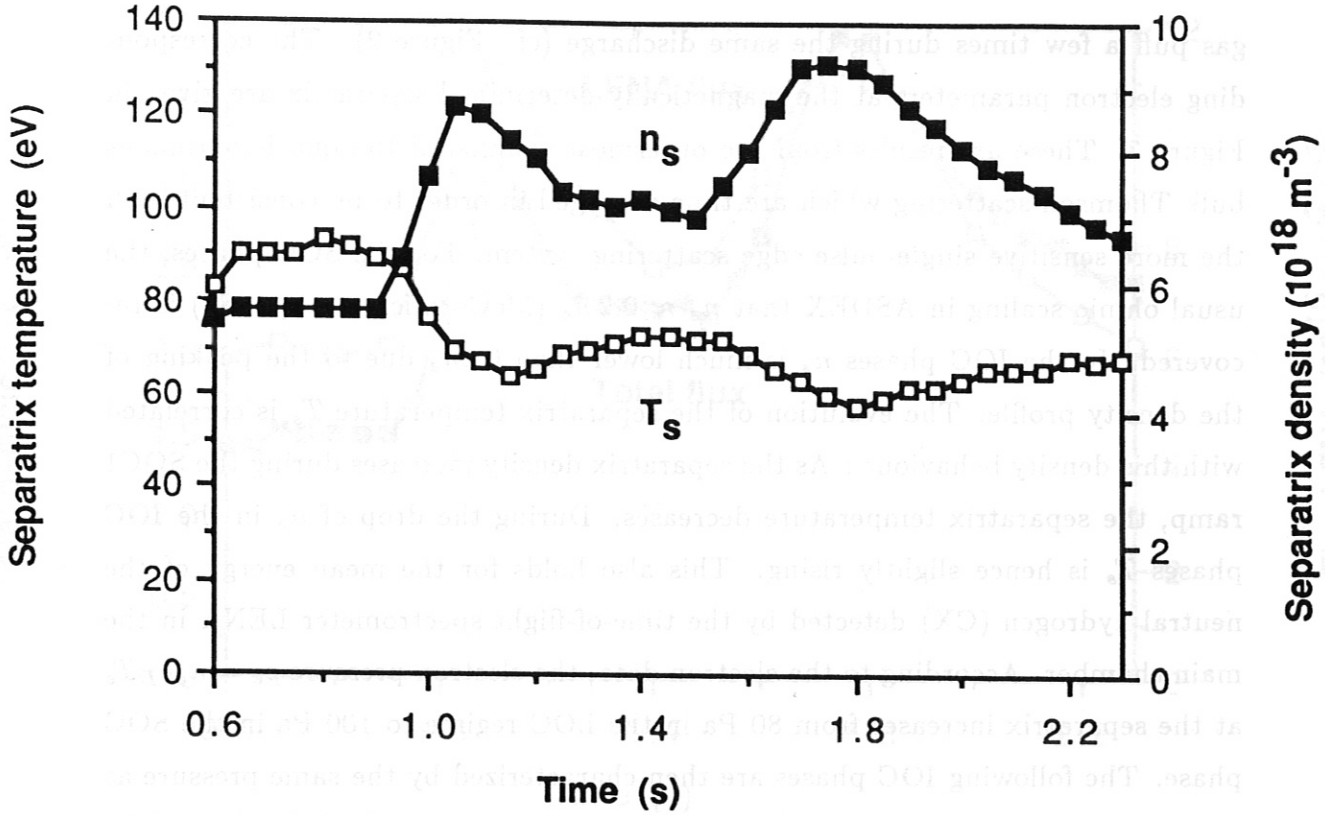

FIGURE 3 : Temporal evolution of the electron data at the nominal separatrix position from Thomson scattering measurements.

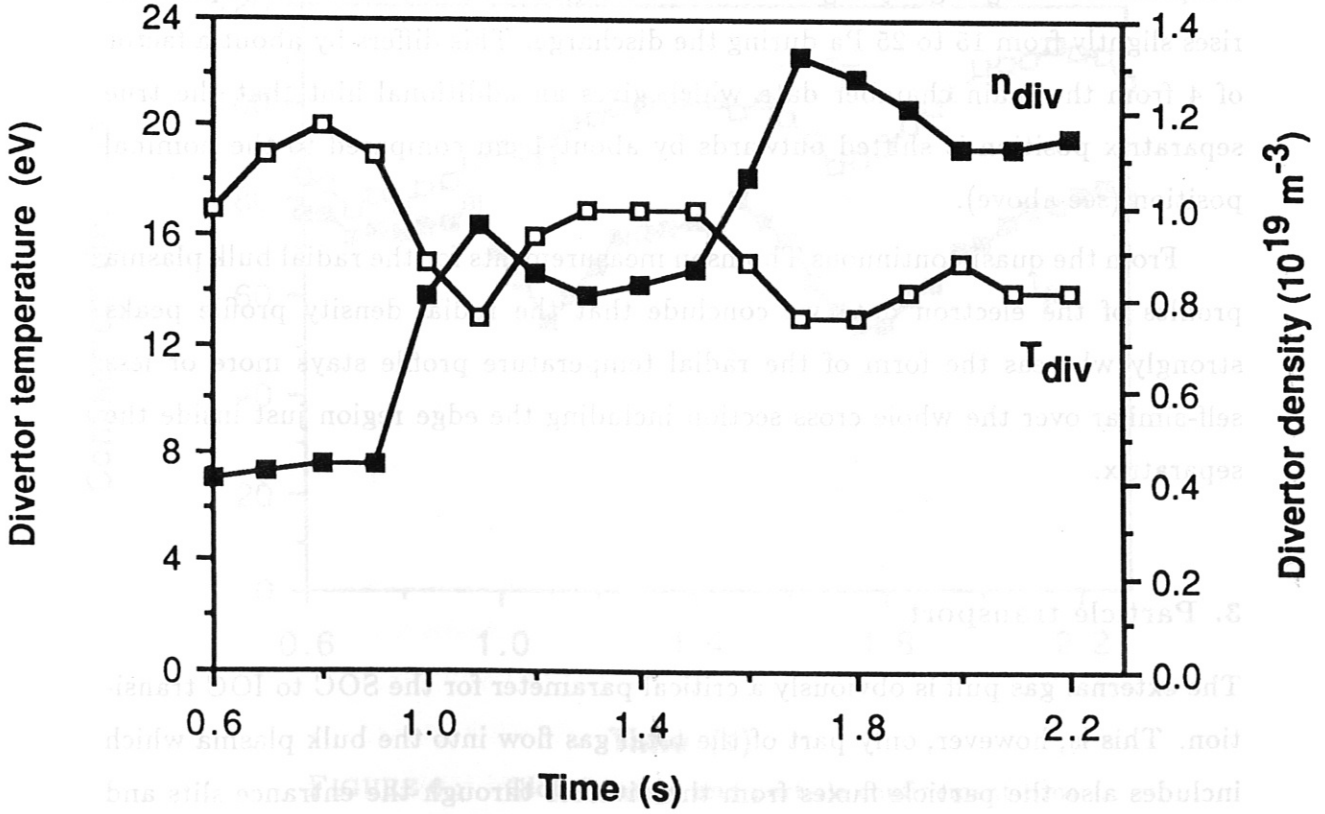

FIGURE 4 : Temporal evolution of the electron data in the divertor chamber from Langmuir probe.

gas puff a few times during the same discharge (cf. Figure 2). The corresponding electron parameters at the magnetically determined separatrix are given in Figure 3. These are results from the outermost channel of the quasi-continuous bulk Thomson scattering which are time-averaged in order to be consistent with the more sensitive single-pulse edge scattering system. For the SOC phases, the usual ohmic scaling in ASDEX that $n_s \approx 0.2\,\overline{n}_e$ (McCormick et al., 1987) is recovered. In the IOC phases n_s is much lower than $0.2\overline{n}_e$ due to the peaking of the density profile. The evolution of the separatrix temperature T_s is correlated with this density behaviour : As the separatrix density increases during the SOC1 ramp, the separatrix temperature decreases. During the drop of n_s in the IOC phases T_s is hence slightly rising. This also holds for the mean energy of the neutral hydrogen (CX) detected by the time-of-flight spectrometer LENA in the main chamber. According to the electron data, the electron pressure $p_e = n_e k_B T_e$ at the separatrix increases from 80 Pa in the LOC regime to 100 Pa in the SOC phase. The following IOC phases are then characterized by the same pressure as in the LOC phase, i.e. 80 Pa at the edge. Figure 5 shows that the behaviour of the electron data in the divertor resembles the separatrix behaviour with the divertor temperature being slightly higher in the IOC regime. There, the electron pressure rises slightly from 15 to 25 Pa during the discharge. This differs by about a factor of 4 from the main chamber data which gives an additional hint that the true separatrix position is shifted outwards by about 1 cm compared to the nominal position (see above).

From the quasi-continuous Thomson measurements for the radial bulk plasma profiles of the electron data we conclude that the radial density profile peaks strongly whereas the form of the radial temperature profile stays more or less self-similar over the whole cross section including the edge region just inside the separatrix.

3. Particle transport

The external gas puff is obviously a critical parameter for the SOC to IOC transition. This is, however, only part of the total gas flow into the bulk plasma which includes also the particle fluxes from the divertor through the entrance slits and

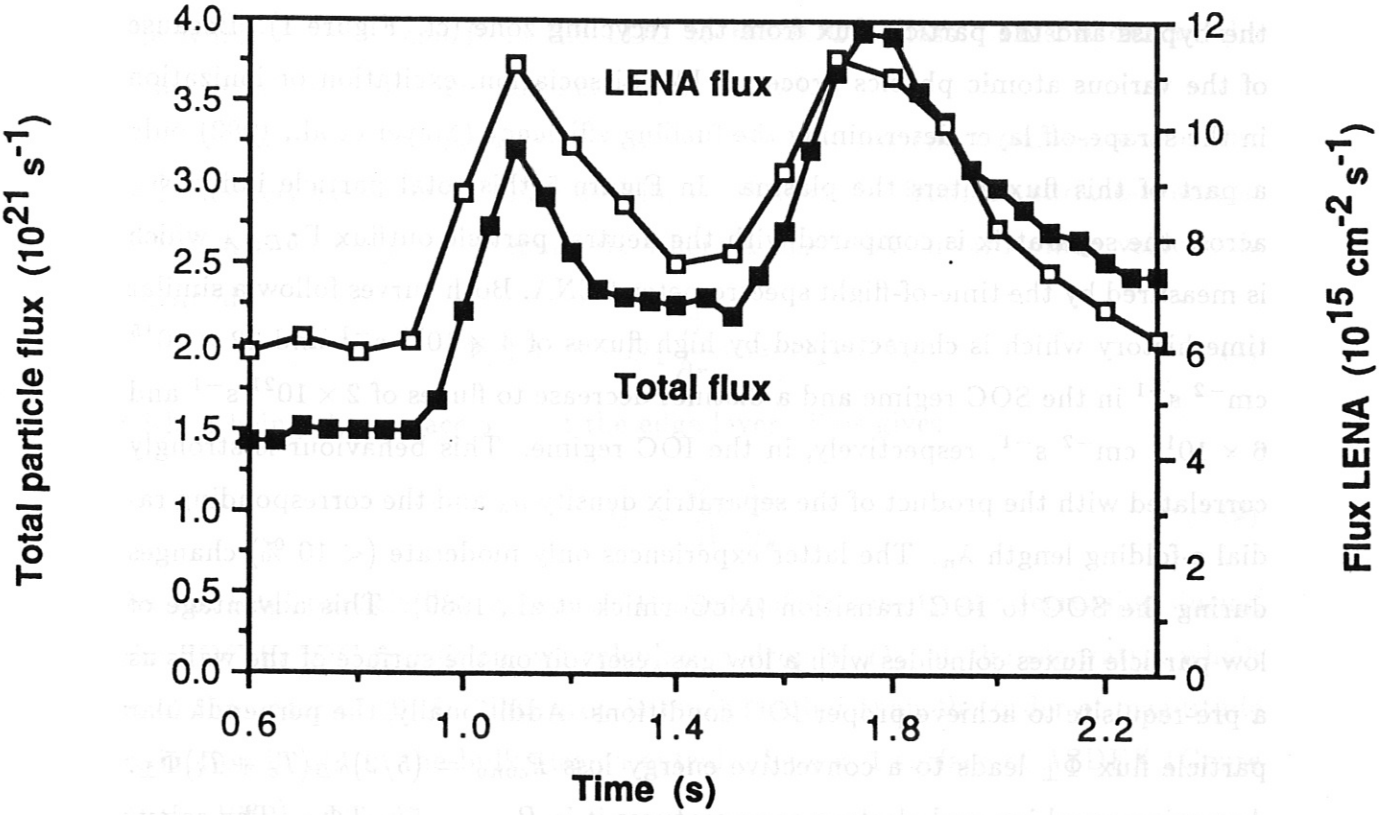

FIGURE 5 : Total hydrogen ion and neutral outflux in the midplane across the separatrix.

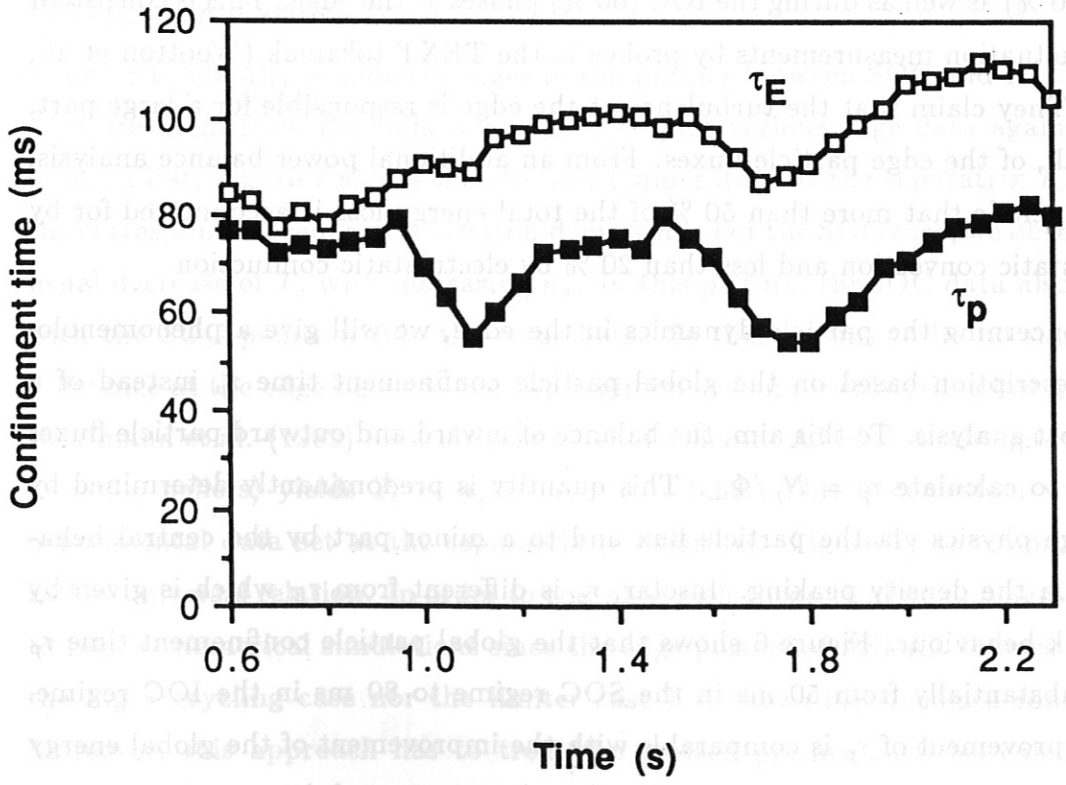

FIGURE 6 : Global energy and particle confinement time.

the bypass and the particle flux from the recycling zone (cf. Figure 1). Because of the various atomic physics processes like dissociation, excitation or ionization in the scrape-off layer determining the fuelling efficiency (Mayer et al., 1982) only a part of this flux enters the plasma. In Figure 5 this total particle influx $\Phi_\perp$ across the separatrix is compared with the neutral particle outflux Γ_{LENA} which is measured by the time-of-flight spectrometer LENA. Both curves follow a similar time history which is characterized by high fluxes of 4×10^{21} s^{-1} and 12×10^{15} cm^{-2} s^{-1} in the SOC regime and a distinct decrease to fluxes of 2×10^{21} s^{-1} and 6×10^{15} cm^{-2} s^{-1}, respectively, in the IOC regime. This behaviour is strongly correlated with the product of the separatrix density n_s and the corresponding radial e-folding length λ_n. The latter experiences only moderate (< 10 %) changes during the SOC to IOC transition (McCormick et al., 1989). This advantage of low particle fluxes coincides with a low gas reservoir on the surface of the walls as a pre-requisite to achieve proper IOC conditions. Additionally, the perpendicular particle flux $\Phi_\perp$ leads to a convective energy loss $P_{conv} = (5/2)k_B(T_e + T_i)\Phi_\perp$. Assuming equal ion and electron temperatures it is $P_{conv} = 5k_BT\Phi_\perp$. The calculations yield the convective energy flux to be the dominant energy loss during the SOC (80 %) as well as during the IOC (60 %) phases at the edge. This is consistent with fluctuation measurements by probes in the TEXT tokamak (Wootton et al., 1988). They claim that the turbulence at the edge is responsible for a large part, if not all, of the edge particle fluxes. From an additional power balance analysis, they conclude that more than 50 % of the total energy loss is accountered for by electrostatic convection and less than 20 % by electrostatic conduction.

Concerning the particle dynamics in the edge, we will give a phenomenological description based on the global particle confinement time τ_p instead of a transport analysis. To this aim, the balance of inward and outward particle fluxes is used to calculate $\tau_p = N_p/\Phi_\perp$. This quantity is predominantly determined by the edge physics via the particle flux and to a minor part by the central behaviour via the density peaking. Insofar, τ_p is different from τ_E which is given by the bulk behaviour. Figure 6 shows that the global particle confinement time τ_p rises substantially from 50 ms in the SOC regime to 80 ms in the IOC regime. The improvement of τ_p is comparable with the improvement of the global energy confinement time τ_E. On the other hand, τ_p is not as much improved as τ_E over

the whole density scan from the LOC to the IOC2 phase. This is due to the dependence of τ_p on edge parameters (see below).

In addition, we figure out the change in the transport parameters at the edge, namely the perpendicular diffusion coefficient $D_\perp$, from the surface-averaged diffusion equation at the separatrix where a negligible inward pinch velocity is assumed

$$\Phi_\perp / A \approx -D_\perp \frac{\partial}{\partial r} n \approx D_\perp n_s / \lambda_n \tag{1}$$

with A being the surface area of the edge layer. This gives

$$D_\perp \approx \frac{\Phi_\perp}{A} \frac{\lambda_n}{n_s}. \tag{2}$$

As the total particle flux as well as the separatrix density are decreasing during the SOC to IOC transition, we calculate a drop of $D_\perp$ at the separatrix which is of the order of 20 %. This drop is much smaller than the order-of-magnitude reduction in $D_\perp$ in the bulk plasma outside the $q = 1$ surface of ASDEX (Gehre et al., 1989).

4. Edge correlations

In order to identify possible changes in the physics between SOC and IOC and to separate them from the bulk behaviour, we plot various edge data against each other. First, Figure 7 shows the electron temperature at the separatrix T_s versus the corresponding separatrix electron density n_s. For the SOC case, we observe the usual decrease of T_s with increasing n_s. In this picture, the IOC data also merge with the SOC points within the error bars. So there seems to be no significant difference at the edge between the two regimes. An empirical scaling law given by Kaufmann et al. (1989) for a large number of different ASDEX discharges (ohmic, L mode, pellets) yields $T_e \sim n_e^{-0.4}$ at $r/a = 0.88$. This is consistent with our experimental data set at the separatrix position (cf. Figure 7) and represents a rather universal relation. In order to compare with theoretical modelling, we have to rely on numerical simulations since the edge plasma of ASDEX follows neither the high recycling case nor the limiter case but shows intermediate conditions. Moreover, this approach has to treat the ionized plasma particles consistently with the neutral hydrogen background. Thus, a one-dimensional hydrodynamic

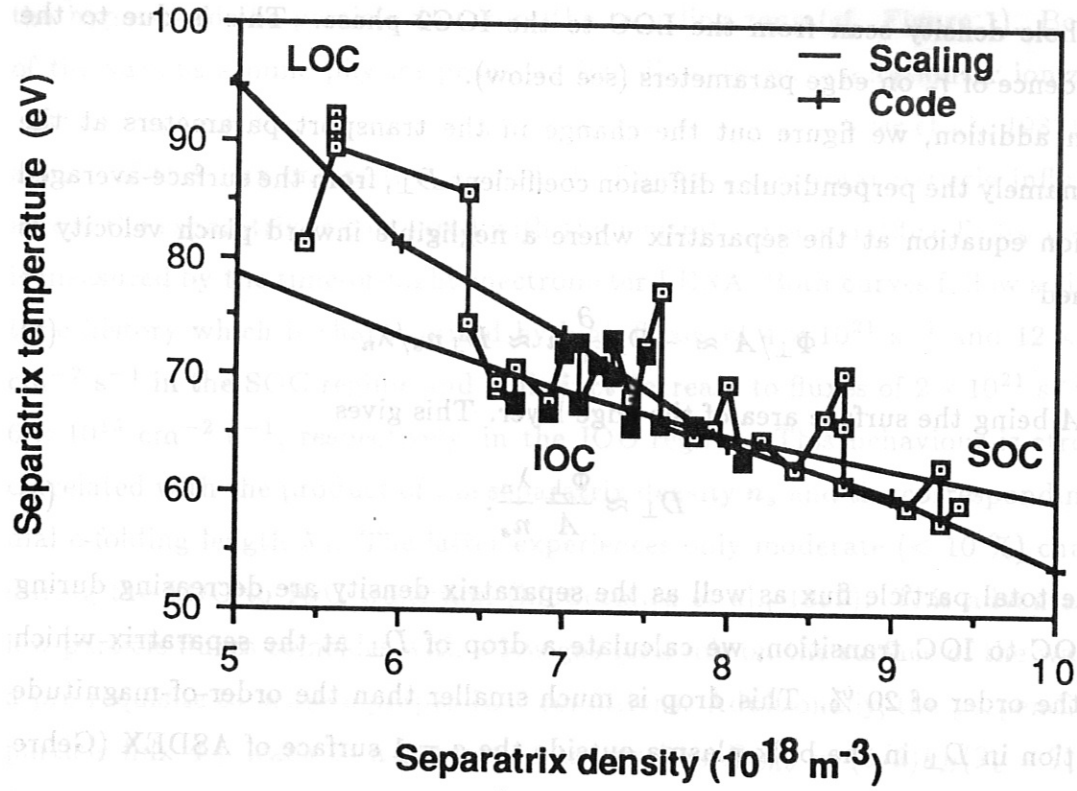

FIGURE 7 : Separatrix temperature versus separatrix density.

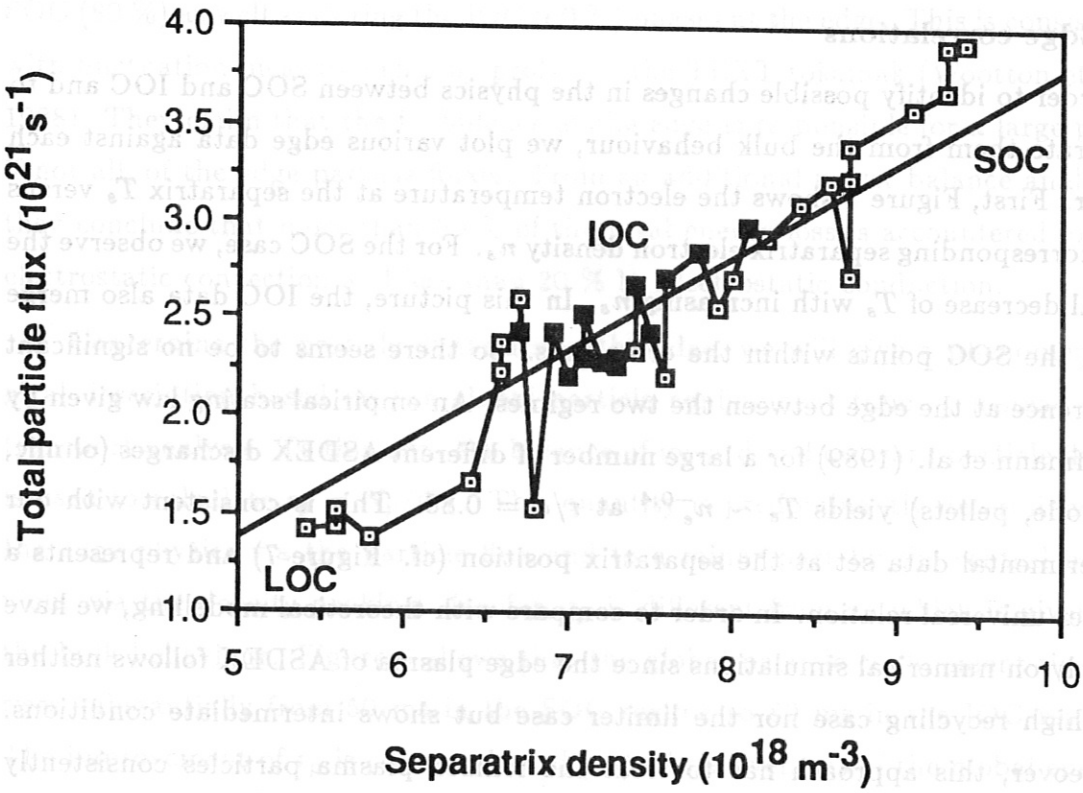

FIGURE 8 : Total particle flux versus separatrix density.

plasma code and a two-dimensional neutral particle Monte-Carlo simulation are coupled and various scenarios are investigated by Schneider et al. (1988). This code then gives also a reasonable fit of the electron data with a good agreement for the relative dependence but a factor of 2 lower temperatures (cf. Figure 7). This may be explained by the 1 cm shift of the separatrix position as determined experimentally (cf. Section 1).

We then discuss the energy confinement time τ_E as a function of the separatrix density n_s. Starting at low densities and low confinement times, τ_E rises proportional to $\overline{n}_e$ and hence n_s in the LOC regime. With larger n_s, τ_E saturates (SOC1) until the gas flux is reduced. Now, n_s drops immediately thus establishing the IOC phase with peaked density profile and with τ_E slowly rising (IOC1). Opening the gas valve results in a sudden drop of the particle as well as the energy confinement. This gives higher densities at the separatrix (SOC2). Then, the gas flux is reduced again. For a second time τ_E goes upwards with decreasing n_s (IOC2) reaching roughly twice the value of the LOC phase.

A similar analysis is performed for the total particle flux $\Phi_\perp$ across the separatrix. The results are shown in Figure 8. This reveals approximately the same linear scaling with the separatrix density from 5 to 10 $\times$ 10^{18} m^{-3} in all phases, i.e. the LOC, the SOC and the IOC. With this scaling and the weak dependence of λ_n on n_s (McCormick et al., 1989) equation (2) is used to derive the corresponding scaling of the perpendicular diffusion coefficient $D_\perp$ with the separatrix density n_s. This yields for the density range from 5 to 10 $\times$ 10^{18} m^{-3} the empirical relation $D_\perp \sim 0.5 - n_s^{-1}$ with $D_\perp$ (m^2/s) and n_s (10^{18} m^{-3}). This has to be compared with an empirical scaling for the diffusion coefficient at the edge with the electron edge parameters as given by Lowry et al. (1988) for JET conditions. They find the best fit as

$$D_\perp \sim T_s^{-0.86}\, n_s^{-0.28}. \qquad (3)$$

This relation yields a 15 % drop of $D_\perp$ during the SOC to IOC transition which is comparable with our estimate (cf. Section 3).

We further illuminate the behaviour of τ_p and τ_E when we correlate them with the corresponding densities, i.e. the separatrix density n_s and the line density $\overline{n}_e$, respectively. Therefore, the ratios τ_p/n_s and $\tau_E/\overline{n}_e$ are plotted in Figure 9. This shows that we reestablish the scalings $\tau_p(n_s)$ and $\tau_E(\overline{n}_e)$ of the LOC phase in the

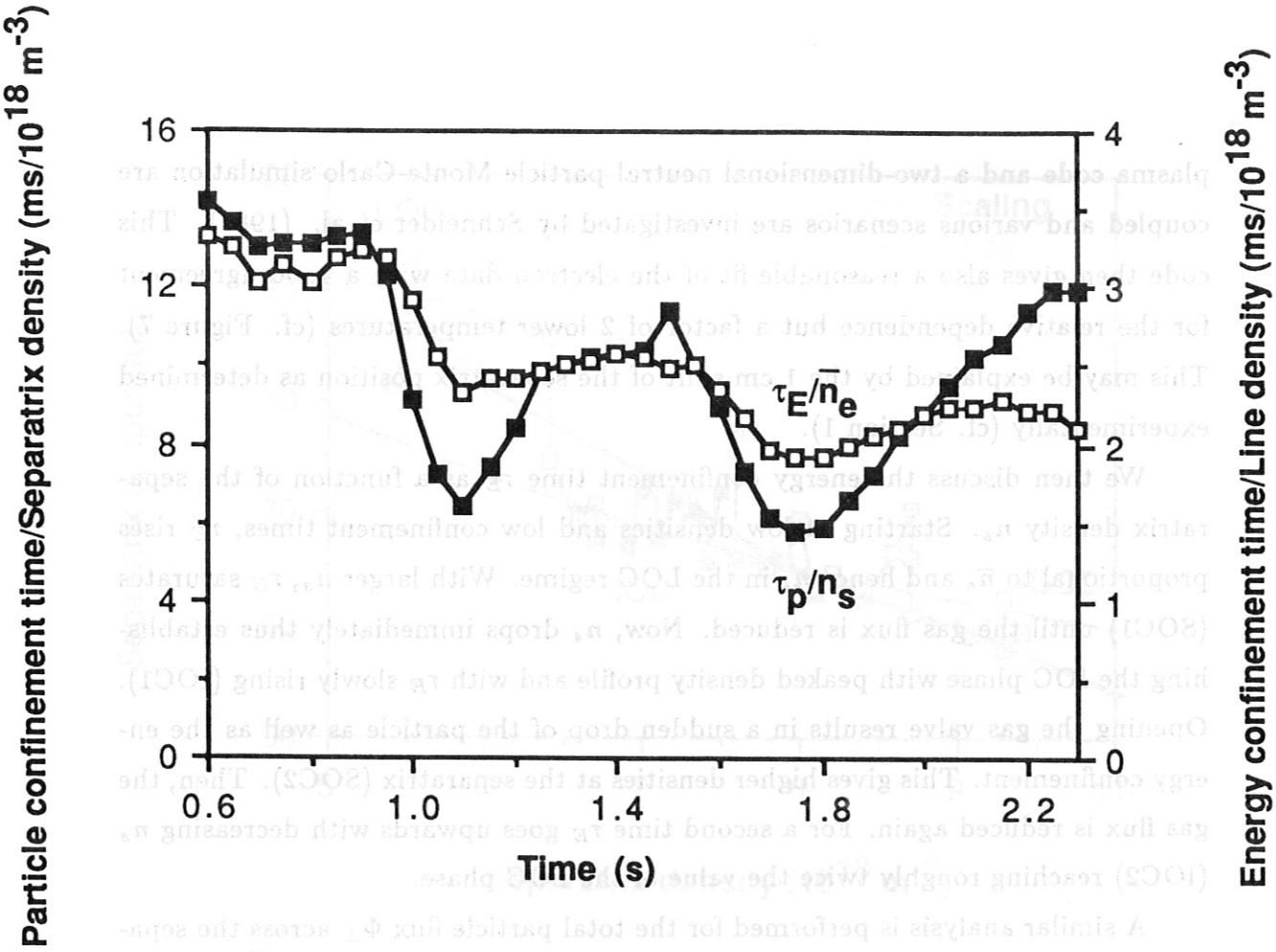

FIGURE 9 : Temporal evolution of the scalings for the particle and the energy confinement.

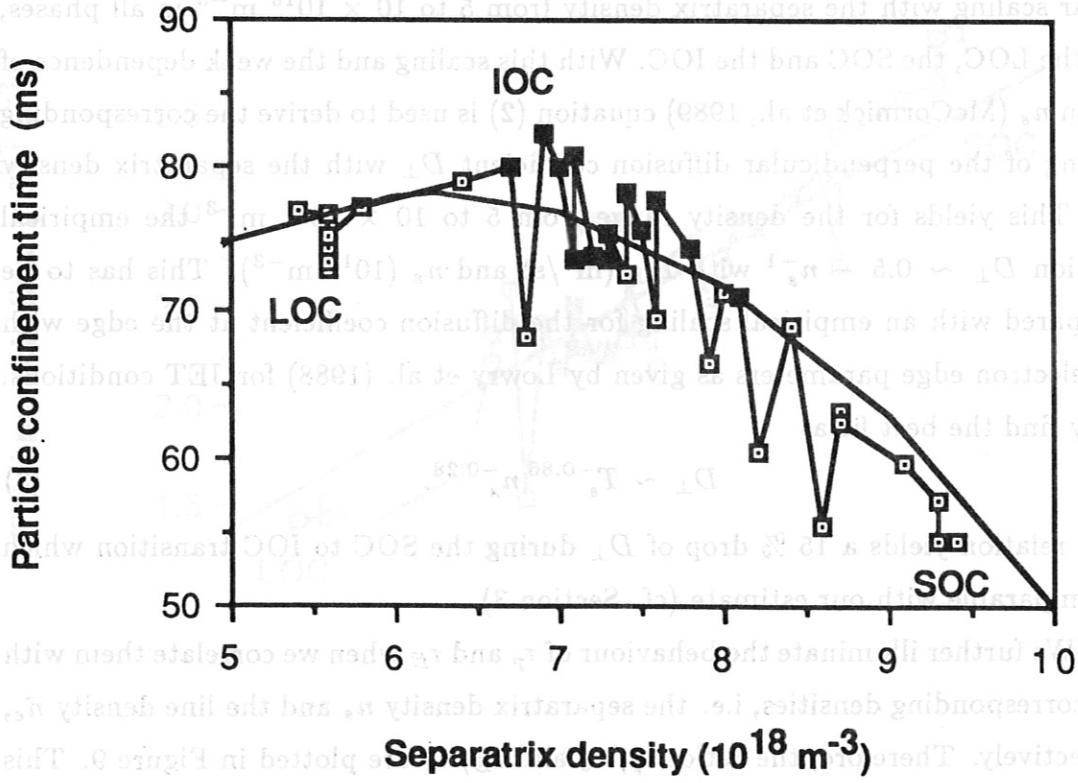

FIGURE 10 : Particle confinement time vs. separatrix density.

final IOC2 phase. The comparison of the IOC and the SOC cases in Figure 9 reveals that the degradation in particle confinement amounts quantitatively to about a factor of two and is a little worse than the degradation in energy confinement.

Furthermore, the regression analysis yields the relation

$$\tau_p = (25 - 2n_s)n_s \tag{4}$$

with τ_p (ms) and n_s (10^{18} m^{-3}). Figure 10 shows this density scaling of the particle confinement time at the periphery of the plasma. For low separatrix density n_s and hence low recycling, τ_p increases with n_s. As the density is further increasing, the recycling at the edge is enhanced and the plasma becomes more and more impervious to penetrating neutrals. Thus, τ_p reaches its maximum value of 80 ms at the critical separatrix density of about 6×10^{18}m^{-3} for ASDEX conditions and decreases for larger values of n_s.

5. Conclusions

The edge plasma in different ohmic confinement regimes of ASDEX is characterized by several experimental diagnostics and modelling. This gives us the temporal as well as the spatial evolution of the edge parameters during the transition from the linear (LOC) to the saturated (SOC) and then to the improved (IOC) ohmic confinement regime. The measurements reveal that the reduction of the external gas feed leads to an immediate drop of the electron density at the separatrix and in the divertor. Correlated with this drop is a slight increase in the electron temperature at these positions. Putting both data together shows that the pressure at the separatrix is approximately the same during the LOC and the IOC phases. Plotting the electron temperature at the separatrix versus the corresponding electron density reveals a universal scaling $T_s \sim n_s^{-0.4}$ for all regimes, i.e. the LOC, the SOC and the IOC data. This experimental result agrees well with two-dimensional edge modelling which is based on an MHD code coupled to a Monte Carlo simulation.

In addition, the total particle flux $\Phi_\perp$ across the separatrix is evaluated from a large number of edge and divertor diagnostics. This particle flux is strongly correlated with the separatrix density n_s and thus shows a sharp decrease in the SOC to IOC transition, too. The flux $\Phi_\perp$ also leads to a convective energy loss across the separatrix. We show that at the periphery of the plasma the convective contribution to the total power losses drops when the confinement is improved. Moreover, the diffusion coefficient $D_\perp$ at the edge is calculated to decrease by about 20 % compared to an order-of-magnitude decrease in the bulk plasma. From the balance of inward and outward particle fluxes, we also evaluate the global particle confinement time τ_p which is mainly determined by the recycling conditions at the periphery of the plasma and to a minor part by the bulk data. In comparison with the particle confinement, the global energy confinement time τ_E is a bulk quantity. In the IOC regime where the proportionality of τ_E with $\overline{n}_e$ is recovered the particle confinement is also enhanced above the SOC values. In addition we are able to give an overall scaling of τ_p with the separatrix density n_s. In the LOC phase, where the separatrix density and hence the recycling remains low, τ_p rises proportional to n_s. This may be partially connected with

the density scaling of the electrostatic turbulence induced particle flux (Rowan et al., 1987). With increasing density the recycling zone is shifted more and more to the scrape-off layer. Thus, τ_p decreases for larger values of n_s. The maximum value between these two extreme cases is obtained at a critical separatrix density of about 6×10^{18} m^{-3} for ASDEX conditions. A similar scaling of τ_p with the line integrated density has also been observed in ALCATOR-A (Marmar, 1978), in JET (Cordey et al., 1984), and in TEXT (Rowan et al., 1987). There, the critical line density is about 20×10^{19}m^{-3}, 1.3×10^{19}m^{-3}, and 4×10^{19}m^{-3}, respectively. For ASDEX, we estimate the critical line density to be 1.5×10^{19}m^{-3}, which fits well these data. In this picture, the LOC values are located at low densities left to the maximum particle confinement and the SOC values are characterized by high separatrix densities far away on the right hand side. Obviously, it is the goal of the IOC regime to adjust the particle recycling such that the critical separatrix density with maximum particle confinement is achieved.

To sum it up, all the results show that the correlation between edge parameters do not change in different ohmic confinement regimes of ASDEX, i.e. the edge physics remains about the same during the LOC, SOC and IOC phases. Improved ohmic confinement is then characterized by an optimum separatrix density which provides a sufficient high temperature in the edge together with low particle fluxes. These optimum conditions then yield the maximum particle confinement.

References

J. G. Cordey, D. V. Bartlett, R. J. Bickerton, G. Bracco, M. Brusati et al., *Proc. 10th IAEA Int. Conf. Plasma Phys. Controlled Nuclear Fusion Research,* London (1984).

O. Gehre, G. Fussmann, K. W. Gentle, and K. Krieger, *Europhys. Conf. Abstr.* **13B** (1989) 167–170.

O. Gehre, O. Gruber, H. D. Murmann, D. E. Roberts, F. Wagner et al., *Phys. Rev. Lett.* **60** (1988) 1502–1505.

G. Haas, W. Poschenrieder, J. Neuhauser, S. Kaesdorf, ASDEX- and NI-Team, *8th Int. Conf. Plasma Surface Interactions in Controlled Fusion Devices,* Jülich (1988).

M. Kaufmann, K. Büchl, G. Fussmann, O. Gehre, K. Grassie et al., *Nucl. Fusion* **28** (1988) 827–848.

M. Kaufmann, W. Sandmann, M. Bessenrodt-Weberpals, K. Büchl, O. Gruber, et al., *Europhys. Conf. Abstr.* **13B** (1989) 47–50.

C. Lowry, P. J. Harbour and J. A. Tagle, *Contrib. Plasma Phys.* **28** (1988) 349–354.

E. S. Marmar, *J. Nucl. Mater.* **76–77** (1978) 59–67.

H.-M. Mayer, F. Wagner, G. Becker, K. Behringer, D. Campbell et al., *J. Nucl. Mater.* **111-112** (1982) 204–210.

K. McCormick, Z. A. Pietrzyk, H. Murmann, M. Lenoci and the ASDEX Team, *J. Nucl. Mater* **145–147** (1987) 215–219.

K. McCormick, Z. A. Pietrzyk, E. Sevillano, G. Haas, H. D. Murmann, H. Verbeek and the ASDEX Team, *Europhys. Conf. Abstr.* **13B** (1989) 895–898.

J. Neuhauser, M. Bessenrodt-Weberpals, B. J. Braams, A. Carlson, R. Chodura et al., *Plasma Phys. Controlled Fusion* (accepted, 1989) .

H. Niedermeyer, G. Becker, B. Bomba, H. Bruhns, K. Büchl et al., *Plasma Phys. Controlled Fusion* **30** (1988) 1443–1453.

W. L. Rowan, C. C. Klepper, C. P. Ritz, R. D. Bengtson, K. W. Gentle et al., *Nucl. Fusion* **27** (1987) 1105–1118.

W. Schneider, J. Neuhauser, G. Haas, K. McCormick, N. Tsois, and R. Wunderlich, *Contrib. Plasma Phys.* **28** (1988) 387–392.

F. X. Söldner, E. R. Müller, F. Wagner, H. S. Bosch, A. Eberhagen et al., *Phys. Rev. Lett.* **61** (1988) 1105–1108.

N. Tsois, M. Bessenrodt-Weberpals, A. Carlson, G. Haas, K. McCormick, et al., *Europhys. Conf. Abstr.* **13B** (1989) 907–910.

A. J. Wootton, M. E. Austin, R. D. Bengtson, J. A. Boedo, R. V. Bravenec et al., *Plasma Phys. Controlled Fusion* **30** (1988) 1479–1491.